JGR Atmospheres

RESEARCH ARTICLE
10.1029/2022JD037612

Changes in Moisture Sources of Atmospheric Rivers Landfalling the Iberian Peninsula With WRF-FLEXPART

J. C. Fernández-Alvarez[1,2], A. Pérez-Alarcón[1,2], J. Eiras-Barca[1,3], A. M. Ramos[4,5], S. Rahimi-Esfarjani[6], R. Nieto[1], and L. Gimeno[1]

[1]Environmental Physics Laboratory (EPhysLab), Centro de Investigación Mariña, Universidade de Vigo, Ourense, Spain, [2]Departamento de Meteorología, Instituto Superior de Tecnologías y Ciencias Aplicadas, Universidad de La Habana, La Habana, Cuba, [3]Defense University Center, The Spanish Naval Academy, Marín, Spain, [4]Institute of Meteorology and Climate Research, Karlsruhe Institute of Technology, Karlsruhe, Germany, [5]Facultade de Ciências, Instituto Dom Luiz (IDL), Universidade de Lisboa, Lisbon, Portugal, [6]Department of Atmospheric and Oceanic Sciences, University of California, Los Angeles, La Jolla, CA, USA

Abstract This paper makes use of a combination of FLEXPART-WRF simulations forced with ERA5 and the CESM2 model—incorporated in the CMIP6 project—to infer a series of changes over the present century in the behavior of the landfalling atmospheric rivers (ARs) arriving to the Iberian Peninsula. In addition, future changes in the intensity and position of their main moisture sources are studied. In overall terms, there is a noticeable increase in the amount of moisture transported by ARs in the study region, particularly accentuated by the end of the century. However, no significant changes in the number of events are observed. A northward shift of both the mean position of the ARs as well as their main sources of moisture is also detected, particularly for the end of the century, and in the summer and fall months. In relation to the latter, an increase in the contribution of moisture contribution is also observed, quantitatively compatible with Clausius-Clapeyron amplification.

Plain Language Summary This paper makes use of a combination of simulations forced with reanalysis data and a climate model to infer a series of changes over the present century in the behavior of the landfalling atmospheric river—ARs, regions of intense moisture transport located in the lower layers of the atmosphere—arriving at the Iberian Peninsula. In addition, future changes in the intensity and position of their main moisture sources are studied. In overall terms, there is a noticeable increase in the amount of moisture transported by ARs in the study region, particularly accentuated by the end of the century. However, no significant changes in the number of events are observed. A northward shift of both the mean position of the ARs as well as their main sources of moisture is also detected, particularly for the end of the century, and in the summer and fall months. In relation to the latter, an increase in the contribution of moisture contribution is also observed, in a ratio similar to that expected.

Key Points:

- FLEXPART-WRF forced with CESM2 model has been able to reproduce the historical conditions of Atmospheric River over the Iberian Peninsula
- A northward shift of the main source regions is projected, notable in summer and fall and particularly by the end of the century
- Gradual strengthening in the intensity of Atmospheric Rivers is expected, observable from an increase in the amount of moisture transported

Supporting Information:

Supporting Information may be found in the online version of this article.

Correspondence to:

J. C. Fernández-Alvarez,
jose.carlos.fernandez.alvarez@uvigo.es

Citation:

Fernández-Alvarez, J. C., Pérez-Alarcón, A., Eiras-Barca, J., Ramos, A. M., Rahimi-Esfarjani, S., Nieto, R., & Gimeno, L. (2023). Changes in moisture sources of atmospheric rivers landfalling the Iberian Peninsula with WRF-FLEXPART. *Journal of Geophysical Research: Atmospheres*, *128*, e2022JD037612. https://doi.org/10.1029/2022JD037612

Received 5 AUG 2022
Accepted 11 APR 2023

1. Introduction

Atmospheric rivers (ARs) are usually defined as narrow corridors—longer than 2,000 km—of anomalous moisture content in the lower levels of the troposphere. They are well known for contributing to the meridional advection of water vapor and latent heat with about 90% of the net transport (Zhu & Newell, 1998). Even though ARs can exist under different meteorological patterns (Gimeno, Algarra, et al., 2021), archetypical ARs are associated with the prefrontal sectors of the storm tracks in the extratropical regions (Gimeno et al., 2014), carrying water intaked by local convergence (Dacre et al., 2015) and particularly by tropical moisture exports mechanism (TME) (e.g., Eiras-Barca et al., 2017; Hu & Dominguez, 2019; Ramos et al., 2016, and others).

ARs account for 20–30% of the total precipitation in southern Europe, particularly in fall and winter months (Eiras-Barca et al., 2021). Even though most ARs may be considered as "beneficial" (Ralph et al., 2019), these phenomena are also the trigger mechanisms of most of the extreme precipitation and flood events over the region in these months (e.g., Eiras-Barca et al., 2016; Ionita et al., 2020; Lavers et al., 2011; Lavers & Villarini, 2013). Thus, ARs are sometimes undeniably responsible for extensive property damage and loss of lives (Dominguez et al., 2018; Gimeno et al., 2016; Ramos et al., 2015).

According to Shukla et al. (2019), a notable increase in the global surface temperature is projected throughout the 21st century. The Clausius-Clapeyron amplification of 7% K^{-1} predicted for the increase in the water holding capacity of the atmosphere has also been projected for the increase in moisture that ARs will be able to carry (Algarra et al., 2020). In addition, it is becoming increasingly clear that the frequency and intensity of extreme precipitation events associated with ARs will be increasing at similar rates (e.g., Espinoza et al., 2018; Lavers & Villarini, 2015, and others). Therefore, there is sufficient evidence in the literature to suggest that as the amount of moisture in the atmosphere increases, its flux will also increase. With a high probability, ARs will tend to increase in intensity in the context of a warmer climate; with a subsequent increase in extreme precipitation events (Lavers et al., 2011). All this in a context of enhanced dynamics in terms of wind modulus (Sousa et al., 2020; Zhang et al., 2019) that will have an impact on human activity and ecosystems.

However, there has not yet been sufficient discussion of future changes in the position of moisture sources, which, by their nature, have the potential to completely modify the spatial distribution of the most active regions of ARs. Thus, albeit indirectly, a potential change in the patterns of moisture sources will lead to a change in the global conditions of meridional transport of energy in the form of latent heat; which will also need to be adequately captured in models that predict the dynamics and thermodynamics of future climate. In this regard, only Algarra et al. (2020) has carried out a global study showing that there has been an increase in anomalous moisture uptake over the period 1980–2017 in regions that are currently considered as moisture sources for ARs. On a regional scale and using water vapor tracing methods, the literature includes some studies such as the one developed by Sodemann and Stohl (2013). These studies show the variability of the sources in the face of different events and as the climate evolves. Additionally, at Nusbaumer and Noone (2018) the CAM5 model is used in combination with water vapor tracers and isotopes to analyze the variability of moisture sources associated with ARs impacting the West Coast of the USA. In general, these studies agree that in future years moisture is expected to be advected from more distant regions for both ARs and similar moisture transport phenomena.

In this regard, not only is the insufficient number of results obtained to date remarkable, but also the low spatial resolution of the findings. Increasing the resolution would provide a better perspective of the physicodynamic processes involved, which could be resolved on a regional scale. Thus, this paper analyzes the expected changes in both the position and relative importance of the different moisture sources feeding the landfalling ARs (LARs) arriving in the Iberian Peninsula under the Coupled Model Intercomparison Project Phase 6 (CMIP6) Socioeconomic Scenario Pathway 5-8.5 (ssp585). For this purpose, a dynamic downscaling methodology that combines the potential of the high-resolution Eulerian mesoscale model Weather Research and Forecast (WRF) with the Lagrangian particle dispersion model FLEXPART has been used. Three sets of simulations of 30 years each were run with WRF initialized with ERA5 or CESM2 as appropriate. Subsequently, these outputs were used to initialize the Lagrangian dispersion FLEXPART-WRF for the same period and to identify the moisture sources in the region of interest.

The area of interest for this study is the Iberian Peninsula, an area that is particularly active in the detection of LARs where they play a relevant role in the hydrological cycle (Eiras-Barca et al., 2021). Likewise, in this region, it has been demonstrated that the socioeconomic impacts of LARs are relevant (Pereira et al., 2016; Trigo et al., 2016; Zêzere et al., 2014).

Beyond presenting a single result of interest for the Iberian Peninsula, this study presents a new methodology that can be replicated in the future under other conditions and in other regions of interest. This methodology—although relatively expensive in computational terms—is reproducible and can provide relevant information to determine the nature of changes in the source regions of moisture associated with ARs and LARs at several locations around the world. This identification is essential for understanding and predicting the actual changes that will occur in these phenomena as well as in the precipitation associated with them.

2. Methods

The main idea of the methodology adopted in this work is as follows: the outputs of the CESM2 model (described below) integrated into the CMIP6 project have been used to initialize high-resolution simulations with the Eulerian mesoscale WRF model for both a historical and two future periods. Later, a detection of ARs located over the North Atlantic with a time-frequency of 6h has been carried out. For this purpose, an innovative methodology based on image analysis (IPART, as detailed in Section 2.3) has been applied. Subsequently, the results of

Table 1
Socioeconomic Scenario Pathways (SSP) and Periods Used in the Analysis

Abbrev.	Scenario	Period
HIST	Historical	1985–2014
MC	ssp585	2036–2065
EC	ssp585	2071–2100

Note. HIST: historical; MC: midcentury; EC: end-century.

these simulations have been used to identify all the LARs events reaching the Iberian Peninsula, and then to operate FLEXPART-WRF (Lagrangian dispersion model) to identify the moisture source regions associated with each of these events; both for the historical period and for the future. This methodology allows us to identify changes in the position and nature of these source regions when the historical and future periods are compared. Details of this methodology and the models used will be described below.

2.1. CESM2 Climate Model (Community Earth System Model Version 2)

Outputs from the Community Earth System Model V2 (CESM2, Danabasoglu et al., 2020) included in the sixth phase of the Coupled Model Intercomparison Project (CMIP6, O'Neill et al., 2016) were used to initialize the simulations. The data were downloaded from the Earth System Grid Federation (ESGF2) at a ≈1° horizontal resolution, and includes 32 vertical levels. Historical data for the period 1985–2014 and future data for midcentury (MC) and end-century (EC) under the ssp585 scenario were used as detailed in Table 1. As discussed in O'Neill et al. (2016), the ssp585 is considered as the "worst-case scenario," with sufficiently high emissions to produce a radiative forcing of 8.5 W m^{-2} which will amplify all signals detected in this analysis.

2.2. Mesoscale Simulations and Lagrangian Dispersions

The Weather Research and Forecast model v3.8.1 (WRF, Skamarock et al., 2019) was used not only to increase the spatial resolution of the simulations but also to lay the necessary basis for carrying out the subsequent Lagrangian particle dispersion. The first simulation was carried out for the HIST period initializing WRF with the fifth generation of the European Reanalysis (ERA5, Hersbach et al., 2020). The WRF simulations initialized with ERA5 (hereinafter referred to as WRF_ERA5) can be considered reliable and will be useful to evaluate the ability of CESM2 to correctly reproduce the atmospheric conditions over the historical period.

Three other sets of simulations were carried out initializing WRF with CESM2. Namely as WRF_CESM2 (HIST) for the historical period, WRF_CESM2 (MC) for midcentury and WRF_CESM2 (EC) for end-century as stated in Table 1. All the aforementioned simulations have been carried out under the same configuration conditions. They consider 40 vertical levels and a horizontal resolution of 20 km in both the simulations forced with ERA5 and CESM2. As for the domain of simulation, the whole North Atlantic Region was considered (115.39°W–42.02°E and 19.41°S–59.51°N, Figure S1 in Supporting Information S1). All simulations preserve time continuity over 30 years and a 1-month spin-up was used. The selected parametrizations were as follows: the WSM6 microphysics scheme (Hong et al., 2006), the Yonsei University PBL scheme (Hong & Lim, 2006), the revised MM5 surface layer scheme (Jiménez et al., 2012), the United Noah Land Surface Model (Tewari et al., 2004), the short and longwave RRTMG schemes (Iacono et al., 2008), and the Kain-Fritsch Ensemble cluster scheme (Kain, 2004). Additionally, a spectral nudging methodology has been applied on waves longer than 1,000 km to avoid the distortion of the large-scale circulation within the regional model domain. These distortions may appear due to the interaction between the model solutions and the boundary conditions (Miguez-Macho et al., 2004). The combination of these parametrizations with spectral nudging has been widely used and tested with very positive results (e.g., Insua-Costa et al., 2019; Insua-Costa & Miguez-Macho, 2018).

The FLEXPART-WRF v3.3.2 model (Brioude et al., 2013) uses the WRF outputs to trigger a Lagrangian dispersion of active moisture tracers—i.e., computational tracers with the ability to solve the mass balance at each iteration. In this case, the FLEXPART-WRF has been forced with WRF_CESM2 with a time step of 6h (FLEX_CESM2). The Hanna Scheme is used to solve the turbulence with convection scheme activated (Hanna, 1984). This parameterization addresses different boundary layer parameters, such as the PBL height, Monin-Obukhov length, convective velocity scale, roughness length and friction velocity (Brioude et al., 2013). FLEXPART-WRF simulations forced with CESM2 are fed with 2 million particles homogeneously distributed over the entire domain (40°E−100°W and 15°S–57°N, see Figure S1 in Supporting Information S1). Additionally, FLEXPART-WRF provides 40 vertical levels and 400 × 777 points available for particle release. The spatial and temporal resolutions

of the outputs are 20 km and 6 hr, respectively. The particles move forward temporally throughout the period of interest, and a biased—rather than Gaussian—turbulence is assumed for them in the convective PBL.

Together with FLEX_CESM2, we conducted analogous simulations forcing FLEXPART-WRF with ERA5 instead of CESM2. This output (herein FLEX_ERA5) may be considered as "control" experiment. As proposed by Stohl and James (2004), at least one particle is guaranteed per point and vertical level. Additionally, the release of particles is also homogeneous in time, starting and ending with the simulation. To evaluate WRF_CESM2 and FLEX_CESM2 configurations; absolute errors (MAE), root mean square errors (RMSE), Pearson's correlations (R), and bias (B) statistics were obtained.

2.3. Detection of Atmospheric Rivers and Tracking of Moisture Sources

For the detection of atmospheric river events, the innovative Image-Processing-based Atmospheric River Tracking (IPART) method is used (Xu et al., 2020). This methodology applies thresholds to the natural spatiotemporal scale of ARs to achieve detection. Thus, the methodology is magnitude-independent and applicable to a Vertical Integrated Moisture Flux (IVT)-based detection. This method has been inspired by the image-processing by reconstruction (THR) technique (Vincent, 1993) and shows a low sensitivity to the choice of parameters that makes it less vulnerable to divergences between present and future climate. The IPART is fed with the IVT outputs in kg m^{-1} s^{-1} obtained from the zonal and meridional components of the water vapor flux, vertically integrated between the 300 and 1,000 hPa levels for both WRF-CESM2 and WRF-ERA5. Levels above 300 hPa have a negligible contribution to the IVT count (Ratna et al., 2016). Subsequently, the IVT fields are decomposed into background and anomaly components and ARs are detected for each time step. An analogous analysis has been carried out with CESM2 data for MC and EC. IPART must be configured with the selection of various detection parameters. The configuration used in this analysis is presented in Table S1 in Supporting Information S1.

With the detection of ARs carried out, LARs affecting the Iberian Peninsula are selected; and the moisture sources identification methodology starts for each period. Months from January to March (JFM), April to June (AMJ), July to September (JAS), and October to December (OND) were independently analyzed. Annual results (ANNUAL) are also provided. For this analysis, the "total AR cross-sectional moisture flux" variable provided by IPART is interpolated to the points considered in the target region at 00, 06, 12, and 18 UTC. If at least one of the considered points provides a nonzero value, the event is used in the subsequent methodology in order to identify its moisture source.

Active tracers dispersion methodology provided by FLEXPART-WRF is applied to each particle that is located over the target region during the detection of an event. The methodology used to identify moisture sources work as follows: changes in specific humidity q along the path described by each particle are estimated as detailed in Equation 1, where m is the mass of the particle and $e - p$ accounts for changes in q—either by evaporation or precipitation processes. Changes are analyzed every 6h.

$$e - p = m\left(\frac{dq}{dt}\right) \tag{1}$$

Once the described operation has been calculated for each individual trajectory of the particles, the total surface freshwater flux on each grid cell can be calculated by assuming the contribution of all trajectories which have traversed the grid area A at a given time (Stohl & James, 2005). The total budget "evaporation minus precipitation" is obtained as detailed in Equation 2, where N is the total number of particles k located over the grid area.

$$E - P = \frac{1}{A}\sum_{k=1}^{N}(e - p)_k \tag{2}$$

The residence time considered in this analysis for following the particles along their trajectory is 10 days (Gimeno, Eiras-Barca et al., 2021; Van Der Ent & Tuinenburg, 2017). Thus, $E - P$—which accounts for the average gains and losses of moisture of particles from day 1 to day 10—are calculated. $E > P$ regions are considered as moisture sources when analyzing particle backward trajectories. This methodology has been used in numerous studies, some of them recent (Cloux et al., 2021; Zhao, 2020). In any case, it should be noted that this methodology is not without limitations; in particular, an overestimation of evaporation and precipitation values associated mainly with nonphysical processes relevant to the phenomenology has been reported (Stohl & James, 2004).

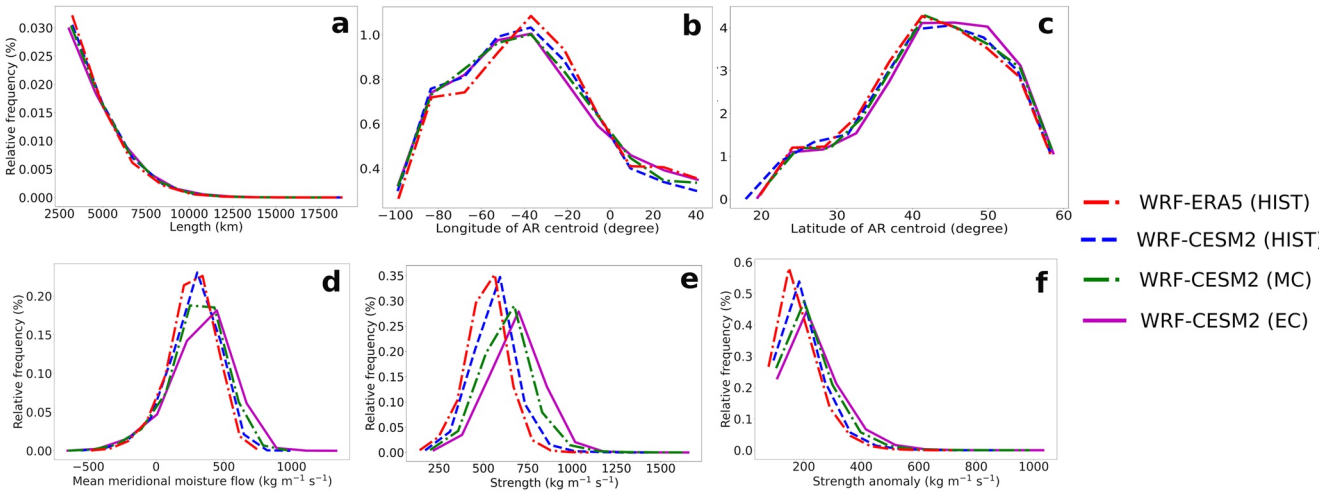

Figure 1. Probability density functions (PDFs) of Weather Research and Forecast (WRF) simulations considered in the analysis for different parameters of interest: (a) atmospheric river (AR) mean length, (b) longitude of AR centroid, (c) latitude of AR centroid, (d) mean meridional moisture flow, (e) AR strength, (f) AR strength anomaly. WRF-ERA5 (HIST) is shown in red dotted lines, WRF-CESM2 (HIST) is shown in blue dotted lines, WRF-CESM2 (MC) is shown in green dotted lines, and WRF-CESM2 (EC) shown in solid purple lines.

It is also noted that the FLEXPART progressively increases the uncertainty of particle trajectories with time (Stohl, 1998). That is, this methodology, although validated and widely used, should continue to be considered as approximation-based.

By choosing only particles (or air cells) implicated in Iberian LAR events, we are able to identify their sources for the desired combination of period, scenario, and simulation. The positive anomaly of the moisture sources is calculated and named anomalous moisture uptake (AMU) following the formalism proposed by Algarra et al. (2020). The AMU is calculated as the difference of the value of the integrated moisture sources $E - P > 0$ for the days with LARs at each grid point and the climatological value of $E - P > 0$ corresponding to that grid point. The climatology for each grid point was calculated as the average for the 30 years of either the seasonal or annual $E - P > 0$ values, regardless of whether a LAR is detected. Finally, the TRansport Of water VApor software (TROVA, Fernández-Alvarez et al., 2022) is used to process the results.

3. Results and Discussion

3.1. North Atlantic ARs Characteristics and Variability

The representation of the characteristics of the ARs and the variability was evaluated considering parameters of structure, intensity, and position of the ARs with probability density functions. Figure 1 and Figure S2 in Supporting Information S1 show the probability density functions (PDFs) of different parameters of interest for ARs landfalling the Iberian Peninsula under all combinations of WRF scenario plus forcings considered in the analysis. WRF-ERA5 (HIST) in red dotted lines and WRF-CESM (HIST) in blue dotted lines are both evaluated under the historical period, forcing WRF with ERA5 in the former and with CESM in the latter. Thus, they are expected to yield similar results if CESM was able to properly reproduce historical conditions. This is actually, in general terms, the result except for the strength (Figure 1e)—where WRF-CESM2 tends to overestimate the integrated water transport in kg m^{-1} s^{-1} when compared to WRF-ERA5—and strength anomaly (Figure 1f) where same conclusions can be obtained.

WRF-CESM2 (MC) in dotted green lines and WRF-CESM2 (EC) in solid purple lines account for the PDFs of WRF simulations forced with CESM in midcentury and end-century years, respectively. These distributions may be compared with WRF-CESM (HIST) to infer changes in the future with respect to the present years. On the whole, a northward displacement of the position of the AR centroids may be expected by the end of the century (Figure 1c). Additionally, a progressive strengthening (Figures 1e and 1f) of the LARs is expected throughout the century according to these results, showing the peak of the distribution of IVT at 750 kg m^{-1} s^{-1} for EC while for the historical period it is close to 500 kg m^{-1} s^{-1}. This progressive reinforcement strengthens the conclusions

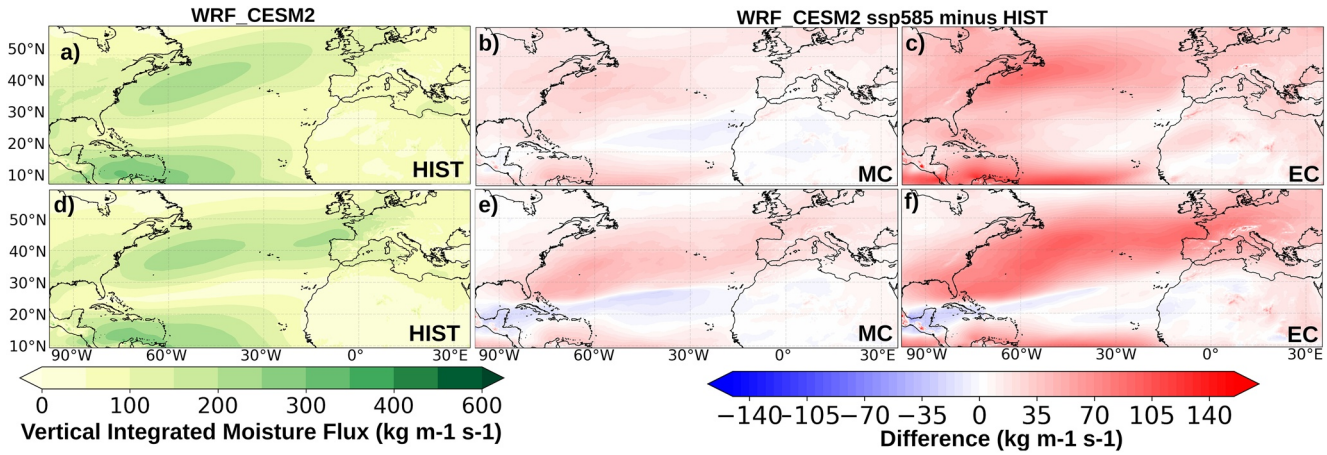

Figure 2. (a) Mean Integrated Moisture Flux (IVT) fields for the historical period. (b) Mean differences in the IVT fields between midcentury (MC) and historical (HIST) periods. (c) Mean differences in the IVT fields EC-Historical. Second row: same as the first row but considering days with landfalling AR (LAR) detection (d–f).

obtained by other studies in recent years. There seems to be a clear consensus that future ARs are expected to be more intense than current ARs in terms of moisture flux (e.g., Zhao, 2020). In addition, it is projected that the mean meridional moisture flux (Figure 1d) for EC will increase with values ranging between 500 and 1,000 kg m^{-1} s^{-1}. However, ARs are projected to be slightly smaller in length for MC and EC (Figure 1a). For the remaining parameters, the changes observed are less significant.

The results presented in Figure 1 project an overall increase in the strength of the ARs for the future. To provide a visual interpretation of this result, Figure 2 shows the mean IVT fields for the historical period and the differences between this and the MC and EC periods for both the climatology as a whole (Figures 2a–2c) and only for the days in which a LAR has been detected over the Iberian Peninsula (Figures 2d–2f). The figure clearly shows an increase in advective dynamics for the future; particularly noticeable in EC and particularly noticeable on LAR days. The strengthening of the ARs presented in Figure 1 is therefore fully compatible with the strengthening of the moisture transport fields observed in Figure 2, where it is also clearly observed that this is particularly intense in the corridors linking the Iberian Peninsula with its moisture sources on LAR days.

Figure 3 shows frequencies of occurrence of AR events—i.e., the relative amount of time steps where the algorithm detected an AR event for each grip point with regard to the total number of time steps considered for the whole period in annual terms—as well as some relevant differences in these frequencies for certain simulations. Particularly, Figure 3a shows the frequency of occurrence in WRF_CESM for the HIST simulation and Figure 3b shows the differences in these frequencies between the former and WRF forced with ERA5. If the degree of coincidence between ERA5 and CESM2 were absolute, no difference should be observed, since both simulations cover the same period. This is not the case, since CESM2 is not expected to reproduce the historical period as accurately as ERA5, but the differences are small and less than 4.5% in all regions, with an overestimation by CESM2 on the eastern U.S. and an underestimation by CESM2 on the North Atlantic corridor. Figures S3a and S3d in Supporting Information S1 provide statistical significance to the differences presented between WRF-CESM2 and WRF-ERA5 for the historical period, highlighting regions that are different in a significant manner with a *t* test significance of 95% and 99%, respectively. It is observed that, in any case, none of the relevant regions for the Iberian Peninsula present statistically significant differences between both sources. Considering, therefore, that this bias between WRF-CESM2 and WRF-ERA5 does not significantly affect the results presented in this manuscript, we do note that it should be taken into account in similar studies that focus on regions such as the east coast of the USA and, to a lesser extent, on the Mediterranean Sea.

Figure 3c shows the frequencies of occurrence of AR events in WRF_CESM2 simulation throughout the MC period, and Figure 3d the differences of the former with the historical period under the same conditions of the simulation. Analogously, Figures 3e and 3f show the same information for the EC period. Two main conclusions can be drawn from these results: on the one hand, it is observed that the pattern of differences is very similar for both periods in structure, but the increases are more marked for EC. On the other hand, there is a clear northward

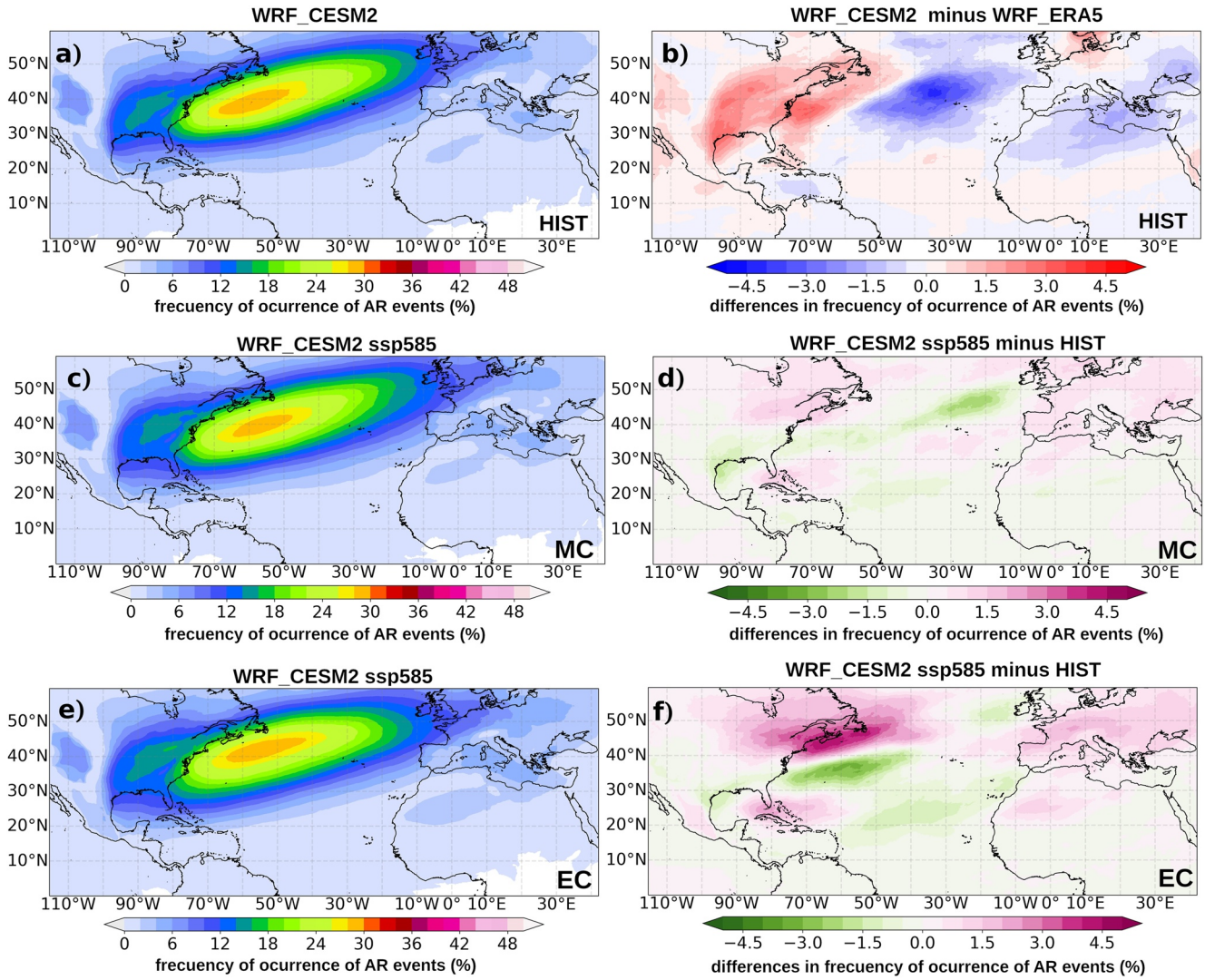

Figure 3. (a) Frequency of occurrence of atmospheric river (AR) events (in % of time steps where an AR has been detected by the Image-Processing-based Atmospheric River Tracking (IPART) out of the total) calculated considering the annual period for WRF_CESM2 (HIST). (b) Differences in frequency of AR events between WRF_CESM2 (HIST) and WRF_ERA5. (c) Same as (a) but for WRF_CESM2 (MC). (d) Differences in frequency of occurrence between WRF_CESM2 (MC) and WRF_CESM2 (HIST). (e) Same as (a) but for WRF_CESM2 (EC). (f) Differences in frequency of occurrence between WRF_CESM2 (EC) and WRF_CESM2 (HIST).

shift in the region of AR activity for the Atlantic coasts of the USA. This shift is particularly marked in EC and may be associated with the poleward shift of the annual mean position of the projected storm track in a warmer climate that has been detected in several generations of coupled climate simulations (Kidston & Gerber, 2010; Miller et al., 2006; Yin, 2005). On the European shores, a certain displacement is also observed, much less marked and in the opposite direction to that observed on the American shores.

In order to add statistical value to the results presented so far, Figure S3 in Supporting Information S1 shows in its second and third columns the points that present statistically significant differences between the time series of the historical period and MC and between the time series of the historical period and EC, respectively. The statistical test used is a *t* test with 95% and 99% significance in the first and second row, respectively. In general, it is observed that for MC the statistically significant differences are restricted to certain tropical regions and to Eastern Europe; as well as to the northwest of the Iberian Peninsula and Northern Italy. In the case of EC, the areas with statistically significant differences increase notably, highlighting a large extension in North America and most of Europe, as well as all of the north of the Iberian Peninsula.

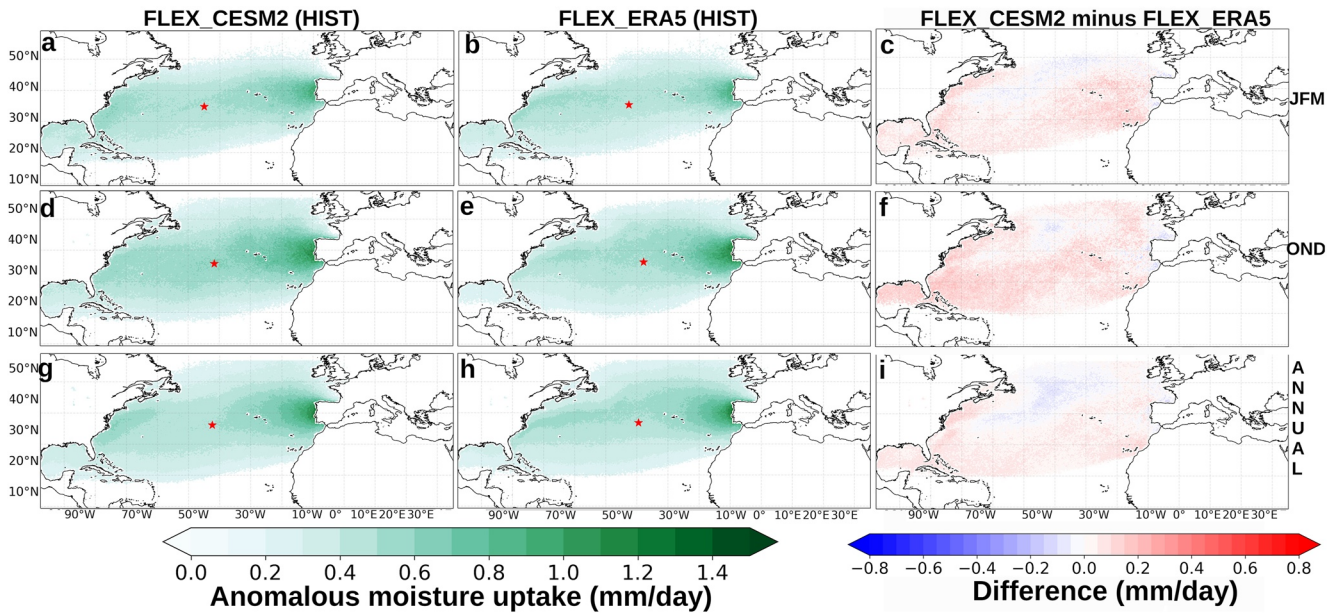

Figure 4. Anomalous moisture uptake (AMU) for FLEX_CESM2 (HIST), FLEX_ERA5 (HIST), and their differences in the first, second, and third columns, respectively. Results are shown for January to March (JFM, a–c), October to December (OND, d–f), and Annual results (ANNUAL, g–i) seasons. Weighted centroids of the AMU patterns are labeled with a red star.

Table S2 in Supporting Information S1 presents statistics of detections of both ARs over the whole domain and LARs over the Iberian Peninsula. It also shows the mean position of the centroid of ARs activity. In this table, it can also be seen how is expected an increase neither in the detections of ARs nor in the detections of LARs—which do not vary significantly between EC and HIST periods—but a displacement of approximately one degree northward in the position of the centroid of activity. This shift is especially marked in JAS, exceeding two degrees of latitude, and practically imperceptible in JFM. That is, most of the observable signal in Figure 3f is attributable to the summer monPerfeths.

3.2. Moisture Sources of Iberian LARs

3.2.1. Moisture Sources Over the Historical Period

Figures S4 and S5 in Supporting Information S1 show the climatology for the moisture sources for the ARs events as described in Section 2.3. These plots have been calculated taking into account all Iberian LAR events for the different periods considered in this analysis using FLEX_CESM2 and FLEX_ERA5 simulations. Specifically, the AMU fields—as detailed in Section 2.3—are shown in Figure 4 and Figure S6 in Supporting Information S1 for the historical simulations on JFM, AMJ, JAS, OND, and ANNUAL separately. These results provide us with a new indicator of the degree of adequacy between the simulations performed with FLEX_CESM2 (HIST) and FLEX_ERA5 (HIST).

The most relevant statistical variables are summarized in Table S3 in Supporting Information S1. In particular, it was found that the value of the value of the Pearson's correlation coefficient R varies in the range of 0.90–0.97, denoting a high temporal correlation between both simulations; mean absolute errors (MAE) ranges from 0.04 to 0.08 mm day^{-1} depending on the season, this in relative terms is a value close to 5% compared to the maximum $E - P > 0$ values, which can be considered relatively low. The same is true for the root mean square error (RMSE), which yields values within the range of 0.05–0.12 mm day^{-1}. The BIAS of the AMU patterns shows discrepancies of about 0.01–0.03 mm day^{-1} when they are compared.

On the other hand, Figure 4 and Figure S6 in Supporting Information S1 show the spatial differences between FLEX_CESM2 and FLEX_ERA5 for the historical period. There is a tendency for FLEX_CESM2 to overestimate the AMU in the central Atlantic and Caribbean Sea regions, although with values below 0.4 mm/day in annual terms throughout the region (Figure 4i).

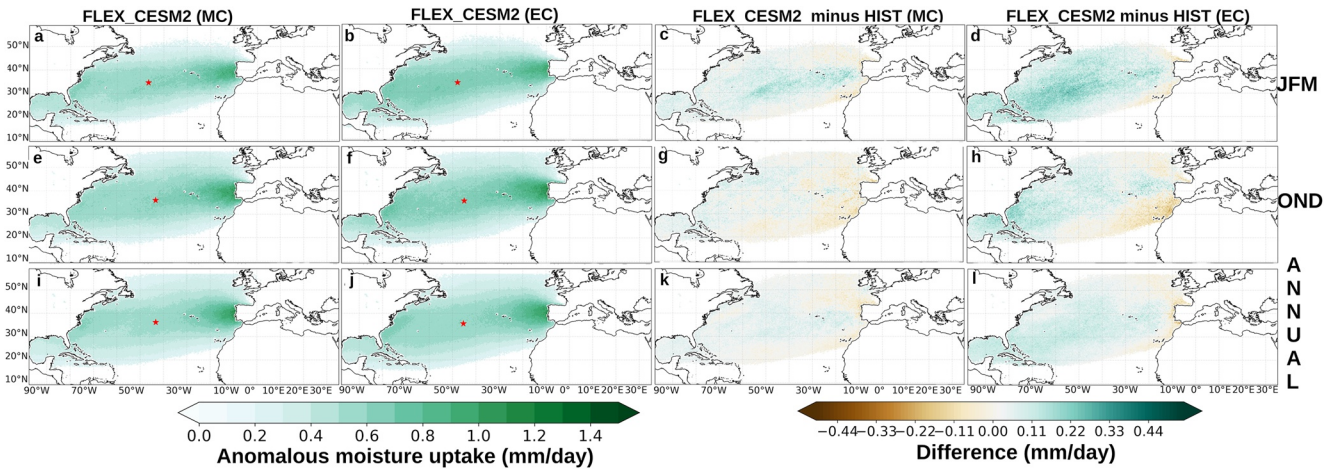

Figure 5. Anomalous moisture uptake for FLEX_CESM2 (midcentury and end-century) and their differences with regard to the historical simulation in the first, second, third, and fourth columns, respectively. Results are shown for January to March (JFM, a–d), October to December (OND, e–h), and Annual results (ANNUAL, i–l) seasons, located in the different rows. Weighted centroids of the anomalous moisture uptake (AMU) patterns are labeled with a red star.

Thus, the results presented in the previous paragraphs show that the representation by FLEX_CESM2 (HIST) for both the moisture sources ($E - P > 0$) and the AMU pattern is realistic when compared to FLEX_ERA5 (HIST). Finally, a relevant feature to compare are the weighted centroids of the AMU patterns. The representation of these centroids allows to analyze the mean positions of the pattern both in present and future climate. These are represented with a red star in Figures 4a, 4b, 4d, 4e, 4g, 4h and Figures S6a, S6b, S6d, S6e, S6g, S6h in Supporting Information S1. Overall, it is observed that the positions are very similar between FLEX_CESM2 (HIST) and FLEX_ERA5 (HIST) for each of the seasons, which is a further indication of the degree of similarity between the two simulations.

3.2.2. Projected Changes in the Moisture Sources

The first two columns in Figure 5 and Figure S7 in Supporting Information S1 show the same results shown in Figure 4 and Figure S6 in Supporting Information S1, but with FLEX_CESM2 for the ssp585 scenario in MC and EC, respectively. The last two columns of these figures show the differences between these simulations and the historical period. It is precisely these last two columns that provide the projections in the foreseeable changes in intensity and position of the source regions where the LARs that affect the Iberian Peninsula would take up moisture anomalously in the medium and long term. In general terms, a gradual increase in the AMU is observed, as well as a northward shift of the regions that act as main sources associated with Iberian LARs. Specifically, Figure 5 shows the expected changes for JFM, OND, and ANNUAL seasons. Figures 5c, 5g, and 5k correspond to MC where an increase is expected above 20°N and located mainly in the central North Atlantic. The opposite is mainly true below 20°N where a slight decrease is expected. For EC, the change pattern signal intensifies with higher values in winter, where the highest anomalous moisture uptakes would be located over the Central and Western Atlantic, the Caribbean Sea, and the Gulf of Mexico. However, for the autumn, the sources are expected to be farther apart because the maximum changes are expected close to the Atlantic coast of the United States. In the annual means, the pattern is very similar but smoother with respect to these seasons. Essentially, a region of lower latitude decrease and upper latitude increase is always observed, which is a robust signal of climate change. For spring, a generally more noticeable decrease is projected for the region between 10°W and 30°W, being of greater intensity for EC (see Figures S7c and S7d in Supporting Information S1). In summer, the increase is mainly projected above 40°N, for source regions located close to the IP (see Figures S7g and S7h in Supporting Information S1). On the other hand, a pattern of moisture sources associated with ARs (Figures S4 and S5 in Supporting Information S1) that is longer in length and organized latitudinally is projected for future periods.

Therefore, in general terms, what is observed is, on the one hand, a reinforcement of the AMU, and on the other hand, a displacement of the AMU toward more southern latitudes. Both signals are particularly clear in the winter months (with an increase of 9% and 24% by MC and EC, respectively) compared to spring months (with an increase of barely 2% for MC and 9% by EC). Particularly noteworthy is the case of summer, showing an increase

Table 2
Projected Seasonal Changes (%) in AMU for MC and EC With Respect to the Historical Patterns

	JFM	AMJ	JAS	OND	ANNUAL
MC	9 (4.5)	2 (1)	17 (8)	3 (1.5)	6 (3)
EC	24 (6)	9 (2.3)	22 (5.5)	9 (2.3)	12 (3)

Note. In parentheses, the percentage change for each degree of temperature that increases for MC and EC under the ssp585 scenario (% K^{-1}).

in the range of 17–22% for MC and EC in the regions with anomalous moisture uptake (see Table 2). These results strengthen the conclusions obtained by the previous studies which state that the contribution of moisture from the sources will increase progressively following a ratio similar to that predicted by the Clausius-Clapeyron amplification of 7% K^{-1} for the maximum amount of moisture that an air cell can contain (Algarra et al., 2020; Bao et al., 2017; Prein et al., 2017). As stated in Table 2, this is particularly observable in winter and summer and is not so clearly evident in the transition months. It is important to note that this increase in the amount of moisture contained in the cells may lead to an increase in precipitation in extreme events, particularly when the orographic and thermodynamic conditions are propitious for it (Algarra et al., 2020; Eiras-Barca et al., 2016, and references therein).

The aforementioned northward shift of the main sources of moisture causes relevant changes in this respect in different regions of the North Atlantic that are worth mentioning. The most significant variations in the position patterns of AMU associated with the Iberian LAR occur in the Central and Western regions of the North Atlantic and in summer in the Cantabrian Sea. Based on these results, the archetypal contribution of moisture from the Gulf of Mexico is expected to be less important throughout the century, as it is gained by the northernmost regions where AMU maxima are located. This behavior is observed in Figure S8 in Supporting Information S1 with the latitudinal displacement of the weighted centroids for the AMU, particularly notable in summer and fall. In the case of winter and annually, a shift of the moisture sources to the west seems to predominate. These displacement results may be associated with the fact that for the future is expected a global increase in water vapor residence time of 3%–6% K^{-1}, lengthening the distance traveled between evaporation and precipitation (Gimeno, Eiras-Barca et al., 2021). Finally, Figure S9 in Supporting Information S1 plots the position of AMU centroids, showing that the greatest displacement to be expected throughout the century is westward in winter months and northward in summer months.

Finally, Figures S10 and S11 in Supporting Information S1 show a statistical significance analysis analogous to those shown so far, but for the AMU both in the form of seasonal and annual means. In summary, it is observed that in winter, autumn and in annual terms, the Gulf of Mexico, western and central Atlantic regions stand out—both for 95% significance and 99% significance—. These statistically significant differences with respect to the historical series are observed for both MC and EC, although they continue to be more accentuated for the latter.

3.3. Limitations and Uncertainties

The limitations and uncertainties associated with this study are mainly related to being restricted to the ssp585 scenario for model forcing. This scenario assumes a development absolutely based on fossil energies that trigger a forcing level of 8.5 W m^{-2}. This scenario is the most pessimistic of all those considered in the CMIP6 and is therefore not the most likely. However, it amplifies the signals and allows us to clearly detect behaviors that in other scenarios, although occurring, would go unnoticed. In any case, it is important to bear in mind that the actual changes will depend on the scenario that finally occurs, and that the real behavior of the projected changes will probably occur with less strength than described in the preceding paragraphs.

Additionally, the detection of ARs (IPART) is dependent on a subjective selection of parameters. These have been selected on the basis of all the literature written on ARs and the researchers' own experience. However, an alternative selection of these parameters would also lead to slightly different results. In addition, the IPART method is sensitive in the interplay between candidate region detection and the subsequent geometric filtering (Xu et al., 2020).

4. Conclusions

Throughout this study, we have made use of a set of simulations that have allowed us to obtain a series of conclusions related to the expected changes in the intensity and position of the main sources of moisture associated with landfalling atmospheric river events over the Iberian Peninsula. First, we conclude that FLEXPART-WRF forced with the CESM2 model included in CMIP6 has been able to reproduce the historical conditions of atmospheric river detection over the Atlantic margin of the Iberian Peninsula. This conclusion has been obtained by comparing its results with those provided by FLEXPART-WRF forced with ERA5, and finding a high degree of similarity

between both. However, there is a westward bias in the frequency of ARs for WRF-CESM2 that—while not significantly affecting the results of this study—could influence the results when analyzing activity involving the east coast of the USA.

Then—and once it was assumed that the FLEXPART-WRF plus CESM2 combination is reliable in relation to the detection of moisture sources—a comparison was made between 30 years of the historical period, 30 years of a midcentury period and 30 years of an end-of-century period assuming the ssp585 scenario. This procedure has allowed inferring the projection of the expected changes in both the strength and distribution of the aforementioned sources.

The most relevant conclusions that this study has obtained in regard to the foreseeable changes that the sources of moisture associated with atmospheric river events over the peninsula will undergo are the following: first, a progressive strengthening of the intensity of the atmospheric rivers reaching the Iberian Peninsula is to be expected, mainly in terms of moisture content, as has been described in the literature previously. Second, a northward shift of the mean position of the AR centroids is also observed, an outcome that has also been predicted by the literature. Third, and in relation to the sources of moisture associated with these events, a progressive increase in the contribution of moisture from the main sources is observed, as well as a northward displacement of these sources—which will result in a relative loss of importance in critical regions for moisture supply, such as the Gulf of México—mainly in the summer and fall months. In addition, a statistical significance of 99% is observed in these changes in moisture sources with respect to the historical period. Finally, it is observed that the increase in moisture input coincides with the values predicted by Clausius-Clapeyron amplification.

Data Availability Statement

The data sets used in this study are freely available on the internet. ERA5 reanalysis data (Hersbach et al., 2020) and CESM2 model outputs (Danabasoglu et al., 2020) are used for the initial and boundary conditions of the WRF-ARW model. In addition, a description of the WRF-ARW model can be consulted in Skamarock et al. (2019) and for FLEXPART-WRF in Brioude et al. (2013). Finally, Image-Processing-based Atmospheric River Tracking (IPART) method (Xu et al., 2020) and TROVA software (Fernández-Alvarez et al., 2022) are used.

Acknowledgments

J. C. Fernández-Alvarez acknowledges the support from the Xunta de Galicia under Grant ED481A-2020/193. A. Pérez-Alarcón acknowledges the PhD Grant from the University of Vigo. J. Eiras-Barca thanks the Defense University Center at the Spanish Naval Academy (CUD-ENM) for the support provided for this research. A.M.R was supported by the Helmholtz "Changing Earth" program. This work is supported by the SETESTRELO project (Grant PID2021-122314OB-I00) funded by the Ministerio de Ciencia, Innovación y Universidades, Spain. Partial support was also obtained from the Xunta de Galicia under Project ED431 C 2021/44 (Programa de Consolidación e Estructuración de Unidades de Investigació Competitivas (Grupos de Referencia Competitiva) and Consellería de Cultura, Educación e Universidade). In addition, this work has been possible thanks to the computing resources and technical support provided by CESGA (Centro de Supercomputación de Galicia) and Red Española de Supercomputación (RES) (AECT-2022-3-0009 and DATA-2021-1-0005). Funding for open access charge: Universidade de Vigo/CISUG.

References

Algarra, I., Nieto, R., Ramos, A. M., Eiras-Barca, J., Trigo, R. M., & Gimeno, L. (2020). Significant increase of global anomalous moisture uptake feeding landfalling atmospheric rivers. *Nature Communications*, *11*(1), 1–7. https://doi.org/10.1038/s41467-020-18876-w

Bao, J., Sherwood, S. C., Alexander, L. V., & Evans, J. P. (2017). Future increases in extreme precipitation exceed observed scaling rates. *Nature Climate Change*, *7*(2), 128–132. https://doi.org/10.1038/nclimate3201

Brioude, J., Arnold, D., Stohl, A., Cassiani, M., Morton, D., Seibert, P., et al. (2013). The Lagrangian particle dispersion model FLEXPART-WRF version 3.1 [software]. Geoscientific Model Development, *6*(6), 1889–1904. https://doi.org/10.5194/gmd-6-1889-2013

Cloux, S., Garaboa-Paz, D., Insua-Costa, D., Miguez-Macho, G., & Pérez-Muñuzuri, V. (2021). Extreme precipitation events in the mediterranean area: Contrasting two different models for moisture source identification. *Hydrology and Earth System Sciences*, *25*(12), 6465–6477. https://doi.org/10.5194/hess-25-6465-2021

Dacre, H. F., Clark, P. A., Martinez-Alvarado, O., Stringer, M. A., & Lavers, D. A. (2015). How do atmospheric rivers form? *Bulletin of the American Meteorological Society*, *96*(8), 1243–1255. https://doi.org/10.1175/BAMS-D-14-00031.1

Danabasoglu, G., Lamarque, J.-F., Bacmeister, J., Bailey, D., DuVivier, A., Edwards, J., et al. (2020). The community Earth system model version 2 (cesm2) [Dataset]. Journal of Advances in Modeling Earth Systems, *12*, e2019MS001916. https://doi.org/10.1029/2019MS001916

Dominguez, F., Dall'Erba, S., Huang, S., Avelino, A., Mehran, A., Hu, H., et al. (2018). Tracking an atmospheric river in a warmer climate: From water vapor to economic impacts. *Earth System Dynamics*, *9*(1), 249–266. https://doi.org/10.5194/esd-9-249-2018

Eiras-Barca, J., Brands, S., & Miguez-Macho, G. (2016). Seasonal variations in north Atlantic atmospheric river activity and associations with anomalous precipitation over the iberian atlantic margin. *Journal of Geophysical Research: Atmospheres*, *121*, 931–948. https://doi.org/10.1002/2015JD023379

Eiras-Barca, J., Dominguez, F., Hu, H., Garaboa-Paz, D., & Miguez-Macho, G. (2017). Evaluation of the moisture sources in two extreme landfalling atmospheric river events using an Eulerian WRF tracers tool. *Earth System Dynamics*, *8*(4), 1247–1261. https://doi.org/10.5194/esd-8-1247-2017

Eiras-Barca, J., Ramos, A. M., Algarra, I., Vázquez, M., Dominguez, F., Miguez-Macho, G., et al. (2021). European West Coast atmospheric rivers: A scale to characterize strength and impacts. *Weather and Climate Extremes*, *31*, 100305. https://doi.org/10.1016/j.wace.2021.100305

Espinoza, V., Waliser, D. E., Guan, B., Lavers, D. A., & Ralph, F. M. (2018). Global analysis of climate change projection effects on atmospheric rivers. *Geophysical Research Letters*, *45*, 4299–4308. https://doi.org/10.1029/2017GL076968

Pérez-Alarcón, A., Nieto, R., & Gimeno, L. (2022). Trova: Transport of water vapor [software]. SoftwareX, *20*, 101228. https://doi.org/10.1016/j.softx.2022.101228

Gimeno, L., Algarra, I., Eiras-Barca, J., Ramos, A. M., & Nieto, R. (2021a). Atmospheric river, a term encompassing different meteorological patterns. *Wiley Interdisciplinary Reviews: Water*, *8*(6), e1558. https://doi.org/10.1002/wat2.1558

Gimeno, L., Dominguez, F., Nieto, R., Trigo, R., Drumond, A., Reason, C. J., et al. (2016). Major mechanisms of atmospheric moisture transport and their role in extreme precipitation events. *Annual Review of Environment and Resources*, *41*(1), 117–141. https://doi.org/10.1146/annurev-environ-110615-085558

Gimeno, L., Eiras-Barca, J., Durán-Quesada, A. M., Dominguez, F., van der Ent, R., Sodemann, H., et al. (2021b). The residence time of water vapour in the atmosphere. *Nature Reviews Earth & Environment*, *2*(8), 558–569. https://doi.org/10.1038/s43017-021-00181-9

Gimeno, L., Nieto, R., Vázquez, M., & Lavers, D. A. (2014). Atmospheric rivers: A mini-review. *Frontiers of Earth Science*, *2*. https://doi.org/10.3389/feart.2014.00002

Hanna, S. (1984). Applications in air pollution modeling. In *Atmospheric turbulence and air pollution modelling* (pp. 275–310). Springer.

Hersbach, H., Bell, B., Berrisford, P., Hirahara, S., Horányi, A., Muñoz-Sabater, J., et al. (2020). The era5 global reanalysis [Dataset]. Quarterly Journal of the Royal Meteorological Society, *146*(730), 1999–2049. https://doi.org/10.1002/qj.3803

Hong, S.-Y., & Lim, J.-O. J. (2006). The WRF single-moment 6-class microphysics scheme (wsm6). *Asia-Pacific Journal of Atmospheric Sciences*, *42*(2), 129–151.

Hong, S.-Y., Noh, Y., & Dudhia, J. (2006). A new vertical diffusion package with an explicit treatment of entrainment processes. *Monthly Weather Review*, *134*(9), 2318–2341. https://doi.org/10.1175/mwr3199.1

Hu, H., & Dominguez, F. (2019). Understanding the role of tropical moisture in atmospheric rivers. *Journal of Geophysical Research: Atmospheres*, *124*, 13826–13842. https://doi.org/10.1029/2019JD030867

Iacono, M. J., Delamere, J. S., Mlawer, E. J., Shephard, M. W., Clough, S. A., & Collins, W. D. (2008). Radiative forcing by long-lived greenhouse gases: Calculations with the AER radiative transfer models. *Journal of Geophysical Research*, *113*, D13103. https://doi.org/10.1029/2008JD009944

Insua-Costa, D., & Miguez-Macho, G. (2018). A new moisture tagging capability in the weather research and forecasting model: Formulation, validation and application to the 2014 great lake-effect snowstorm. *Earth System Dynamics*, *9*(1), 167–185. https://doi.org/10.5194/esd-9-167-2018

Insua-Costa, D., Miguez-Macho, G., & Llasat, M. C. (2019). Local and remote moisture sources for extreme precipitation: A study of the two catastrophic 1982 Western Mediterranean episodes. *Hydrology and Earth System Sciences*, *23*(9), 3885–3900. https://doi.org/10.5194/hess-23-3885-2019

Ionita, M., Nagavciuc, V., & Guan, B. (2020). Rivers in the sky, flooding on the ground: The role of atmospheric rivers in inland flooding in central Europe. *Hydrology and Earth System Sciences*, *24*(11), 5125–5147. https://doi.org/10.5194/hess-24-5125-2020

Jiménez, P. A., Dudhia, J., González-Rouco, J. F., Navarro, J., Montávez, J. P., & García-Bustamante, E. (2012). A revised scheme for the WRF surface layer formulation. *Monthly Weather Review*, *140*(3), 898–918. https://doi.org/10.1175/mwr-d-11-00056.1

Kain, J. S. (2004). The Kain-Fritsch convective parameterization: An update. *Journal of Applied Meteorology*, *43*(1), 170–181. https://doi.org/10.1175/1520-0450(2004)043<0170:TKCPAU>2.0.CO;2

Kidston, J., & Gerber, E. (2010). Intermodel variability of the poleward shift of the austral jet stream in the CMIP3 integrations linked to biases in 20th century climatology. *Geophysical Research Letters*, *37*, L09708. https://doi.org/10.1029/2010GL042873

Lavers, D. A., Allan, R. P., Wood, E. F., Villarini, G., Brayshaw, D. J., & Wade, A. J. (2011). Winter floods in Britain are connected to atmospheric rivers. *Geophysical Research Letters*, *38*, L23803. https://doi.org/10.1029/2011GL049783

Lavers, D. A., & Villarini, G. (2013). The nexus between atmospheric rivers and extreme precipitation across Europe. *Geophysical Research Letters*, *40*, 3259–3264. https://doi.org/10.1002/grl.50636

Lavers, D. A., & Villarini, G. (2015). The contribution of atmospheric rivers to precipitation in Europe and the United States. *Journal of Hydrology*, *522*, 382–390. https://doi.org/10.1016/j.jhydrol.2014.12.010

Miguez-Macho, G., Stenchikov, G. L., & Robock, A. (2004). Spectral nudging to eliminate the effects of domain position and geometry in regional climate model simulations. *Journal of Geophysical Research*, *109*(D13), 1097. https://doi.org/10.1029/2003JD004495

Miller, R., Schmidt, G., & Shindell, D. (2006). Forced annular variations in the 20th century intergovernmental panel on climate change fourth assessment report models. *Journal of Geophysical Research*, *111*, D18101. https://doi.org/10.1029/2005JD006323

Nusbaumer, J., & Noone, D. (2018). Numerical evaluation of the modern and future origins of atmospheric river moisture over the west coast of the United States. *Journal of Geophysical Research: Atmospheres*, *123*, 6423–6442. https://doi.org/10.1029/2017JD028081

O'Neill, B. C., Tebaldi, C., Van Vuuren, D. P., Eyring, V., Friedlingstein, P., Hurtt, G., et al. (2016). The scenario model intercomparison project (ScenarioMip) for cmip6. *Geoscientific Model Development*, *9*(9), 3461–3482. https://doi.org/10.5194/gmd-9-3461-2016

Pereira, S., Ramos, A. M., Zêzere, J. L., Trigo, R. M., & Vaquero, J. (2016). Spatial impact and triggering conditions of the exceptional hydro-geomorphological event of December 1909 in Iberia. *Natural Hazards and Earth System Sciences*, *16*(2), 371–390. https://doi.org/10.5194/nhess-16-371-2016

Prein, A. F., Liu, C., Ikeda, K., Trier, S. B., Rasmussen, R. M., Holland, G. J., & Clark, M. P. (2017). Increased rainfall volume from future convective storms in the us. *Nature Climate Change*, *7*(12), 880–884. https://doi.org/10.1038/s41558-017-0007-7

Ralph, F. M., Rutz, J. J., Cordeira, J. M., Dettinger, M., Anderson, M., Reynolds, D., et al. (2019). A scale to characterize the strength and impacts of atmospheric rivers. *Bulletin of the American Meteorological Society*, *100*(2), 269–289. https://doi.org/10.1175/BAMS-D-18-0023.1

Ramos, A. M., Nieto, R., Tomé, R., Gimeno, L., Trigo, R. M., Liberato, M. L., & Lavers, D. A. (2016). Atmospheric rivers moisture sources from a Lagrangian perspective. *Earth System Dynamics*, *7*(2), 371–384. https://doi.org/10.5194/esd-7-371-2016

Ramos, A. M., Trigo, R. M., Liberato, M. L., & Tomé, R. (2015). Daily precipitation extreme events in the iberian peninsula and its association with atmospheric rivers. *Journal of Hydrometeorology*, *16*(2), 579–597. https://doi.org/10.1175/JHM-D-14-0103.1

Ratna, S. B., Cherchi, A., Joseph, P., Behera, S., Abish, B., & Masina, S. (2016). Moisture variability over the indo-pacific region and its influence on the indian summer monsoon rainfall. *Climate Dynamics*, *46*(3–4), 949–965. https://doi.org/10.1007/s00382-015-2624-z

Shukla, P. R., Skeg, J., Buendia, E. C., Masson-Delmotte, V., Pörtner, H.-O., Roberts, D., et al. (2019). *Climate change and land: An IPCC special report on climate change, desertification, land degradation, sustainable land management, food security, and greenhouse gas fluxes in terrestrial ecosystems*.Intergovernmental Panel on Climate Change.

Skamarock, W. C., Klemp, J. B., Dudhia, J., Gill, D. O., Liu, Z., Berner, J., et al. (2019). A description of the advanced research WRF model version 4 [Software]. National Center for Atmospheric Research, *145*. https://doi.org/10.5065/1dfh-6p97

Sodemann, H., & Stohl, A. (2013). Moisture origin and meridional transport in atmospheric rivers and their association with multiple cyclones. *Monthly Weather Review*, *141*(8), 2850–2868. https://doi.org/10.1175/MWR-D-12-00256.1

Sousa, P. M., Ramos, A. M., Raible, C. C., Messmer, M., Tomé, R., Pinto, J. G., & Trigo, R. M. (2020). North Atlantic integrated water vapor transport—From 850 to 2100 ce: Impacts on Western European rainfall. *Journal of Climate*, *33*(1), 263–279. https://doi.org/10.1175/JCLI-D-19-0348.1

Stohl, A. (1998). Computation, accuracy and applications of trajectories—A review and bibliography. *Atmospheric Environment*, *32*(6), 947–966.

Stohl, A., & James, P. (2004). A Lagrangian analysis of the atmospheric branch of the global water cycle. part i: Method description, validation, and demonstration for the august 2002 flooding in central Europe. *Journal of Hydrometeorology*, *5*(4), 656–678. https://doi.org/10.1175/1525-7541(2004)005<0656:ALAOTA>2.0.CO;2

Stohl, A., & James, P. (2005). A Lagrangian analysis of the atmospheric branch of the global water cycle. part ii: Moisture transports between Earth's ocean basins and river catchments. *Journal of Hydrometeorology*, *6*(6), 961–984. https://doi.org/10.1175/JHM470.1

Tewari, M., Chen, F., Wang, W., Dudhia, J., LeMone, M., Mitchell, K., et al. (2004). Implementation and verification of the unified Noah land surface model in the WRF model. In *20th conference on weather analysis and forecasting/16th conference on numerical weather prediction* (Vol. 1115, pp. 2165–2170). American Meteorological Society.

Trigo, R. M., Ramos, C., Pereira, S. S., Ramos, A. M., Zêzere, J. L., & Liberato, M. L. (2016). The deadliest storm of the 20th century striking Portugal: Flood impacts and atmospheric circulation. *Journal of Hydrology*, *541*, 597–610. https://doi.org/10.1016/j.jhydrol.2015.10.036

Van Der Ent, R. J., & Tuinenburg, O. A. (2017). The residence time of water in the atmosphere revisited. *Hydrology and Earth System Sciences*, *21*(2), 779–790. https://doi.org/10.5194/hess-21-779-2017

Vincent, L. (1993). Morphological grayscale reconstruction in image analysis: Applications and efficient algorithms. *IEEE Transactions on Image Processing*, *2*(2), 176–201. https://doi.org/10.1109/83.217222

Xu, G., Ma, X., Chang, P., & Wang, L. (2020). Image-processing-based atmospheric river tracking method version 1 (ipart-1) [software]. Geoscientific Model Development, *13*(10), 4639–4662. https://doi.org/10.5194/GMD-13-4639-2020

Yin, J. H. (2005). A consistent poleward shift of the storm tracks in simulations of 21st century climate. *Geophysical Research Letters*, *32*, L18701. https://doi.org/10.1029/2005GL023684

Zêzere, J. L., Pereira, S., Tavares, A., Bateira, C., Trigo, R., Quaresma, I., et al. (2014). Disaster: A GIS database on hydro-geomorphologic disasters in Portugal. *Natural Hazards*, *72*(2), 503–532. https://doi.org/10.1007/s11069-013-1018-y

Zhang, Z., Ralph, F. M., & Zheng, M. (2019). The relationship between extratropical cyclone strength and atmospheric river intensity and position. *Geophysical Research Letters*, *46*, 1814–1823. https://doi.org/10.1029/2018GL079071

Zhao, M. (2020). Simulations of atmospheric rivers, their variability, and response to global warming using GFDL's new high-resolution general circulation model. *Journal of Climate*, *33*(23), 10287–10303. https://doi.org/10.1175/JCLI-D-20-0241.1

Zhu, Y., & Newell, R. E. (1998). A proposed algorithm for moisture fluxes from atmospheric rivers. *Monthly Weather Review*, *126*(3), 725–735. https://doi.org/10.1175/1520-0493(1998)126<0725:APAFMF>2.0.CO;2